Dyes and Pigments 80 (2009) 279–286

Contents lists available at ScienceDirect

Dyes and Pigments

journal homepage: www.elsevier.com/locate/dyepig

An experimental and computational study of intramolecular charge transfer: Diarylamino derivatives of 7*H*-benzimidazo(2,1-*a*)benz(*d*,*e*)isoquinolin-7-ones

Wei Jiang [a], Jinan Tang [a], Qi Qi [a], Yueming Sun [a,*], Hengyun Ye [b], Dawei Fu [b]

[a] School of Chemistry and Chemical Engineering, Southeast University, Nanjing 210096, PR China
[b] Ordered Matter Science Research Center, College of Chemistry and Chemical Engineering, Southeast University, Nanjing 210096, PR China

ARTICLE INFO

Article history:
Received 17 May 2008
Received in revised form 1 July 2008
Accepted 3 July 2008
Available online 23 July 2008

Keywords:
7*H*-Benzimidazo(2,1-*a*)-benz(*d*,*e*)isoquinolin-7-ones
Photophysical
X-ray
Isomer
Charge transfer
DFT

ABSTRACT

A novel intramolecular donor–acceptor system of four isomers consisting of 7*H*-benzimidazo(2,1-*a*)benz(*d*,*e*)isoquinolin-7-ones and diarylamine units was synthesized and characterized; the absorption and fluorescence spectra of the system in a variety of solvents were investigated. Intramolecular charge transfer was confirmed within the system by virtue of shifts in emission maximum with increasing solvent polarity; a high dipole moment for the intramolecular excited state was calculated using the Lippert equation. Shorter lifetimes were observed in polar solvents compared with those in non-polar solvents, indicating strong dipole–dipole interactions occurred. The ground-state geometry, lowest energy transition and the UV–vis spectrum of the system were studied using density functional theory and time-dependent density functional theory at B3LYP/6-31G* level, which showed that the calculated outcomes were in good agreement with experimental data.

1. Introduction

π-Conjugated compounds with donor–acceptor architectures are currently of interest because the built-in intramolecular charge transfer can facilitate ready manipulation of the electronic structure (HOMO/LUMO levels), leading to small band gap semiconducting [1–3] materials with enhanced third-order nonlinear optical properties [4,5]. Though design and synthesis of new architectures, donor–acceptor conjugated compounds can extend to systems with efficient photoinduced charge transfer and separation for photovoltaic devices [6,7] and to bipolar charge transport materials for light-emitting diodes [8–10], lasers [11,12], and other applications [13–15].

In the field of organic light-emitting diodes (OLED), diarylamines are ideal electron donors with high carrier mobility, high thermal and photochemical stability, and these properties are commonly used as hole-transporting materials for balanced charge injection and transport in LED devices [16–19]. On the other hand, naphthalimide is an excellent electron accepting chromophore, which has often been used for constructing materials for green or yellow light emission [20–25]. However, the poor nucleophilic assistance of the nonbonding electron pair on the nitrogen has made difficult its incorporation into aromatic systems by classical methods, requiring severe reaction condition. Several synthetic strategies to obtain arylamine derivatives by using Cu/bronze [26] or palladium catalyst [27] have been published. It is well known that 1,8-naphthalimide derivatives are very sensitive to their surroundings and their absorption and emission spectra are frequently affected by the nature of the solvent. Here, we have incorporated diarylamine into the naphthalimide chromophore and synthesized four novel isomers **1a**–**2b**, 3- and 4-diphenylamino-7*H*-benzimidazo(2,1-*a*)benz(*d*,*e*)isoquinolin-7-ones (**1a** and **1b**) and 3- and 4-(2-naphthylphenylamino)-7*H*-benzimidazo(2,1-*a*)benz(*d*,*e*)isoquinolin-7-ones (**2a** and **2b**). The structures are shown in Fig. 1. The absorption and emission spectra are examined. The broad range of emissions may indicate the formation of a charge-transfer state. In this work, the influence of solvents with various polarities upon absorption and emission spectra was investigated and the charge transfer phenomenon in these compounds was systematically studied.

2. Experimental

2.1. Materials and methods

Melting points were determined on a digital melting point apparatus WRS-1 made in Shanghai and uncorrected. IR spectra were recorded on a 5DX-FT-2 spectrophotometer using KBr pellets.

* Corresponding author. Tel.: +86 25 52090619; fax: +86 25 52090621.
E-mail address: sun@seu.edu.cn (Y. Sun).

0143-7208/$ – see front matter © 2008 Elsevier Ltd. All rights reserved.
doi:10.1016/j.dyepig.2008.07.009

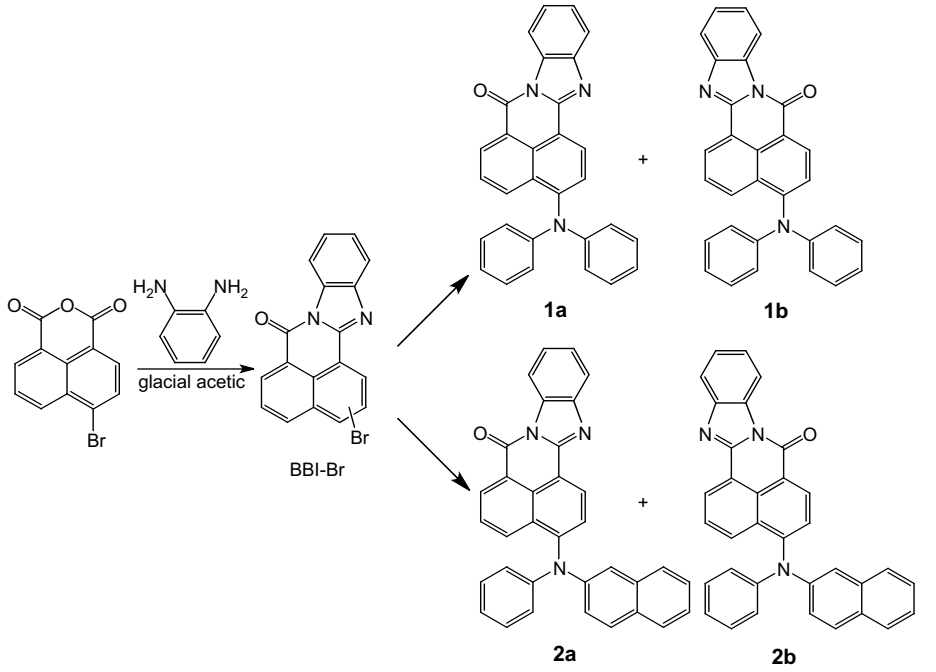

Fig. 1. Synthetic route of isomers **1a**–**2b**.

^{1}H NMR and ^{13}C NMR spectra were recorded on Bruker (ARX-300) spectrophotometer (300 MHz) in $CDCl_3$ and using TMS as internal standard (chemical shifts are given as δ in ppm). The mass spectra were recorded on ZAB-HS spectrometer. Elemental analyses were performed on Elementar Vario MICRO. UV–vis aborption spectra were recorded using a Hitachi U-300 spectrophotometer, while photoluminescent spectra were a Hitachi F-4050. The quantum yields for emission were measured at room temperature with fluorescein (in 0.1 M NaOH, quantum yield = 0.93) as the standard. The lifetime was measured by nano-second laser system. All reactions were monitored by thin-layer chromatography. Common reagents grade chemicals are commercially available and were used without further purification.

2.2. Synthesis

The synthetic route was shown in Fig. 1.

2.2.1. Method 1. Palladium-catalyzed synthesis

To a two-necked flask under nitrogen were added 3- and 4-Br-7*H*-benzimidazo(2,1-*a*)benz(*d*,*e*)isoquinolin-7-ones (1 mmol), diarylamine (1.2 mmol), $Pd(OAC)_2$ (0.020 mmol), tri-*tert*-butyl phosphine (0.04 mmol), and sodium *tert*-butoxide (1.5 mmol). Toluene (3 mL) was then added to the flask via a syringe. The resulting mixture was stirred for 4–6 h at 120 °C. After cooling, to the mixture was added water (3 mL) and then ethyl acetate (20 mL). The organic layer was separated from the aqueous layer, washed with water and brine solution, and dried over anhydrous magnesium sulfate. Evaporation of the solvent under reduced pressure afforded the crude solid. Purification on a silica gel column using a petroleun ether/ethyl acetate mixture as the eluent gave the desired pure product **1a** (**2a**) and **1b** (**2b**), respectively.

2.2.2. Method 2. Copper-catalyzed synthesis

A mixture of 3- and 4-Br-7*H*-benzimidazo(2,1-*a*)benz(*d*,*e*)isoquinolin-7-ones (1 mmol), diarylamine (1.2 mmol), potassium carbonate (2.0 mmol), copper(I) iodide (0.05 mmol), 18-crown-6 (0.05 mmol) and 3 mL *o*-dichlorobenzene was heated to 190 °C for 24–30 h under nitrogen. After cooling, the mixture was dissolved with chloroform and water, the organic layer was washed successively with water and brine solution, and dried over anhydrous magnesium sulfate, the crude solid was further purified by silica gel column using a petroleun ether/ethyl acetate mixture as the eluent gave the desired pure product **1a** (**2a**) and **1b** (**2b**), respectively.

*2.2.2.1. Compound **1a**.* Mp: 269–270 °C; ^{1}H NMR (300 MHz, $CDCl_3$, TMS): δ 8.82 (d, J = 8.0 Hz, 1H), 8.75 (d, J = 7.5 Hz, 1H), 8.59–8.56 (m, 1H), 8.38 (d, J = 8.7 Hz, 1H), 7.90–7.87 (m, 1H), 7.64 (t, J = 7.4 Hz, 1H), 7.50–7.45 (m, 3H), 7.31–7.25 (m, 5H), 7.09–7.04 (m, 5H); ^{13}C NMR ($CDCl_3$): δ 160.76, 148.49, 132.45, 131.92, 129.58, 129.23, 129.19, 128.29, 126.71, 126.55, 125.88, 125.22, 123.64, 123.52, 123.40, 119.64, 115.86; IR (KBr, cm^{-1}) 1691, 1654, 1398, 1348, 1236; MS

Table 1
Crystal data and structure refinement for **1a** and **1b**

	1a	**1b**
Formula	$C_{30}H_{19}N_3O$	$C_{30}H_{19}N_3O$
FW	437.48	437.48
Crystal system	Monoclinic	Monoclinic
Space group	*P*2(1)/*c*	*P*2(1)/*n*
a (Å)	8.0827(8)	8.111(8)
b (Å)	23.3632(19)	13.355(12)
c (Å)	11.5857(13)	20.406(19)
α (deg)	90	90
β (deg)	94.413(8)	98.352(15)
γ (deg)	90	90
Z	4	4
V	2181.3(4)	2187(3)
D_{calc} (g cm^{-3})	1.332	1.329
T (K)	293(2)	293(2)
Radiation λ (Å)	Mo Kα (0.71073)	Mo Kα (0.71073)
μ (mm^{-1})	0.082	0.082
$R(I > 2\sigma(I))$	0.0584	0.1301
Goodness-of-fit on F^2	1.005	1.286
Largest difference peak and hole (e Å^3)	0.166/−0.185	1.121/−0.412

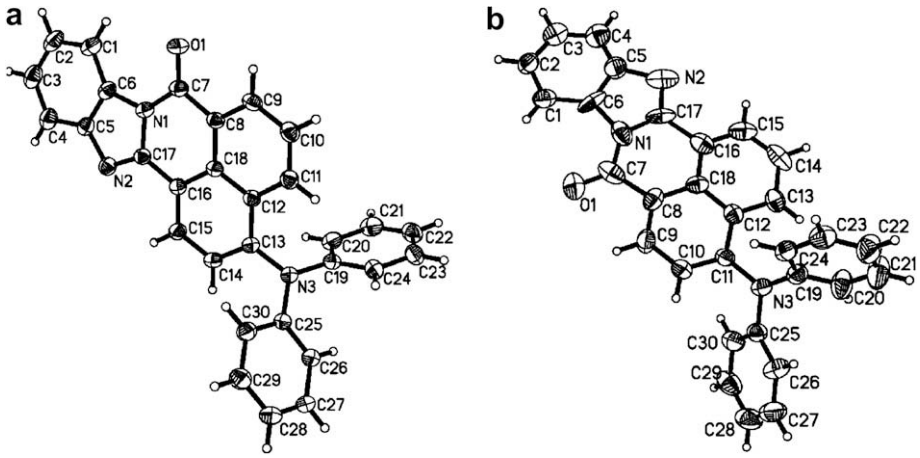

Fig. 2. ORTEP diagrams of **1a** and **1b**.

(70 eV) *m*/*z* 437 (M^+); Anal. calcd for $C_{30}H_{19}N_3O$: C 82.38, H 4.35, N 9.61; found C 82.35, H 4.50, N 9.55.

2.2.2.2. Compound ***1b***. Mp: 252–253 °C; ^{1}H NMR (300 MHz, $CDCl_3$, TMS): δ 8.83 (d, J = 7.2 Hz, 1H), 8.72 (d, J = 8.1 Hz, 1H), 8.60–8.57 (m, 1H), 8.18 (d, J = 8.5 Hz, 1H), 7.91–7.88 (m, 1H), 7.58 (t, J = 7.7, 8.1 Hz, 1H), 7.50–7.43 (m, 3H), 7.32–7.27 (m, 5H), 7.13–7.07 (m, 5H); ^{13}C NMR ($CDCl_3$): δ 160.30, 152.28, 148.48, 132.77, 129.65, 129.44, 129.39, 128.45, 127.45, 126.69, 125.77, 125.36, 124.09, 123.92, 119.75, 118.87, 115.95; IR (KBr, cm^{-1}) 1699, 1651, 1367, 1238; MS (70 eV) *m*/*z* 437 (M^+); Anal. calcd for $C_{30}H_{19}N_3O$: C 82.38, H 4.35, N 9.61; found C 82.20, H 4.32, N 9.48.

2.2.2.3. Compound ***2a***. Mp: >300 °C; ^{1}H NMR (300 MHz, $CDCl_3$, TMS): δ 8.83 (d, J = 7.8 Hz, 1H), 8.76 (d, J = 7.0 Hz, 1H), 8.58–8.54 (m, 1H), 8.42 (d, J = 8.2 Hz, 1H), 7.89–7.85 (m, 1H), 7.80 (d, J = 8.2 Hz, 2H), 7.59–7.48 (m, 5H), 7.41–7.27 (m, 6H), 7.16–7.13 (m, 3H); ^{13}C NMR ($CDCl_3$): δ 164.70, 164.27, 151.51, 148.72, 146.33, 135.83, 134.66, 132.11, 131.91, 131.27, 130.81, 130.12, 129.99, 129.75, 129.17, 128.54, 128.49, 127.51, 127.12, 126.86, 126.10, 125.60, 124.52, 124.40, 124.02, 123.84, 120.81, 119.47; IR (KBr, cm^{-1}) 1710, 1658, 1432, 1311, 1220; MS (70 eV) *m*/*z* 487 (M^+); Anal. calcd for $C_{34}H_{21}N_3O$: C 82.78, H 4.31, N 8.62; found C 82.75, H 4.35, N 8.52.

2.2.2.4 Compound ***2b***. Mp: >300 °C; ^{1}H NMR (300 MHz, $CDCl_3$, TMS): δ 8.78 (d, J = 7.2 Hz, 1H), 8.70 (d, J = 8.1 Hz, 1H), 8.58–8.55 (m, 1H), 8.21 (d, J = 8.5 Hz, 1H), 7.90–7.87 (m, 1H), 7.81 (t, J = 8.7 Hz, 2H), 7.60 (t, J = 3.7, 5.2 Hz, 1H), 7.53–7.46 (m, 4H), 7.42–7.39 (m, 3H), 7.35–7.30 (m, 3H), 7.15–7.12 (m, 3H); ^{13}C NMR ($CDCl_3$): δ 164.71, 152.47, 150.38, 144.86, 136.37, 135.42, 132.06, 132.04, 131.32, 131.50, 130.25, 130.02, 129.66, 129.10, 129.08, 127.58, 127.74, 127.28, 126.85, 126.78, 126.44, 126.35, 123.82, 123.65, 123.40, 123.35, 118.95; IR (KBr, cm^{-1}) 1700, 1654, 1532, 1344, 1224; MS (70 eV) *m*/*z* 487 (M^+); Anal. calcd for $C_{34}H_{21}N_3O$: C 82.78, H 4.31, N 8.62; found C 82.70, H 4.30, N 9.57.

2.3. Crystallography

Suitable monocrystals of **1a** and **1b** were obtained by slow evaporation of its methanol solution. All the measurements were made on a MERCURY CCD diffractometer by the ω scan technique at room temperature using graphite-monochromated Mo Kα radiation. The structures were solved by direct methods and refined by full-maxtrix least-squares procedures on F^2 (SHELXL-97). All non-hydrogen atoms were refined anisotropically. The crystal and experimental data are shown in Table 1.

2.4. Quantum mechanical calculations

The structure of **1a** and **1b** was optimized by semiempirical density functional theory (DFT) [28] using a B3LYP/6-31G* basis set. The HOMO and LUMO frontier orbitals of compound NA-CZ-1 were calculated by TD-DFT methods at the B3LYP/6-31G* level. The structure optimization and energy calculations were performed with the GAUSSIAN 98 program.

Table 2
Selected bond lengths (Å) and angles (deg) for **1a** and **1b**

1a		**1b**	
Bond lengths	Bond angles	Bond lengths	Bond angles
O1–C7 = 1.216(2)	N1–C17–N2 = 112.96(16)	O1–C7 = 1.216(8)	N1–C17–N2 = 120.8(7)
N2–C17 = 1.301(2)	C7–N1–C17 = 125.26(16)	N2–C17 = 1.312(8)	C7–N1–C17 = 130.7(7)
N1–C7 = 1.397(2)	O1–C7–N1 = 120.38(18)	N1–C7 = 1.314(9)	O1–C7–N1 = 124.0(8)
N3–C13 = 1.424(2)	C17–N2–C5 = 105.23(16)	N3–C11 = 1.420(7)	C17–N2–C5 = 101.1(7)
N3–C25 = 1.420(2)	C4–C5–N2 = 128.66(19)	N3–C25 = 1.425(7)	C4–C5–N2 = 129.9(8)
N2–C5 = 1.390(2)	N2–C17–C16 = 127.71(16)	N2–C5 = 1.509(10)	N2–C17–C16 = 122.0(7)
N1–C6 = 1.404(2)	C7–N1–C6 = 128.94(15)	N1–C6 = 1.425(8)	C7–N1–C6 = 126.1(7)
N1–C17 = 1.403(2)	O1–C7–C8 = 124.72(18)	N1–C17 = 1.355(9)	O1–C7–C8 = 125.0(7)
N3–C19 = 1.425(2)	N1–C6–C5 = 104.76(16)	N3–C19 = 1.445(7)	N1–C6–C5 = 108.9(7)
	C6–C5–N2 = 111.32(17)		C6–C5–N2 = 106.6(7)
	N1–C17–C16 = 119.32(16)		N1–C17–C16 = 117.2(5)
	C17–N1–C6 = 105.73(15)		C17–N1–C6 = 102.6(7)
	N1–C7–C8 = 114.89(15)		N1–C7–C8 = 111.1(7)
	N1–C6–C1 = 132.9(2)		N1–C6–C1 = 132.1(8)

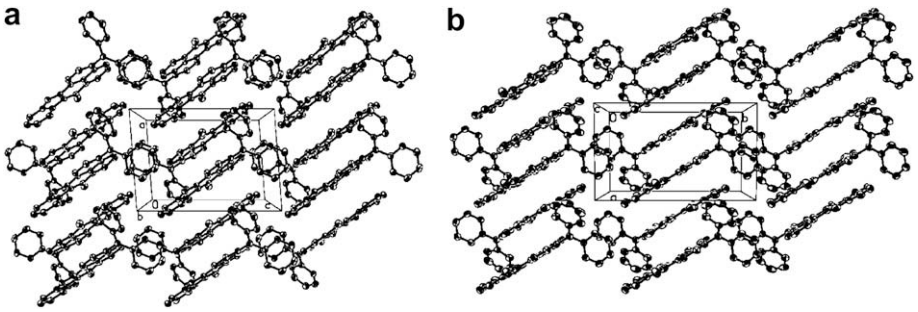

Fig. 3. Packing structure of **1a** and **1b**.

3. Results and discussion

3.1. Synthesis of 7H-benzimidazo(2,1-a)benz(d,e)isoquinolin-7-one isomers

The route to the synthesis of the target isomers is presented in Fig. 1. The isomeric mixture 3- and 4-Br-7*H*-benzimidazo(2,1-*a*)benz(*d*,*e*)isoquinolin-7-ones was synthesized according to methods previously described [29]. The reaction of 4-bromo-1,8-naphthalic anhydride in 1:1 molar ratio with *o*-phenylenediamine in boiling glacial acetic for 5 h, giving a golden yellow solid in good yield (>95%). The isomeric mixture showed single spot on TLC. However, the ^{1}H NMR (300 MHz) was able to assign the differences. From the integration ratio of the proton resonance peaks, the ratio of isomeric mixture is about 1.25:1.

The target isomers **1a**–**2b** were obtained by nucleophilic substitution of the bromide in isomeric 3- and 4-Br-7*H*-benzimidazo(2,1-*a*)benz(*d*,*e*)isoquinolin-7-ones with diarylamine group under copper- and palladium-catalyzed conditions. The isomeric mixture showed two spots on TLC, which can be purified by chromatography onto silica gel columns, respectively. Using a standard set of reaction conditions (CuI/18-crown-6/K_2CO_3/*o*-dichlorobenzene, 190 °C), we obtain the desired pure isomers in 12–18% yield, respectively. Various parameters such as catalyst precursors, base, ligands, and solvents were examined but no better results were obtained. The use of a Pd/P(*t*-Bu)$_3$ catalyst system was first reported by Koie and a modified system was used by Yamamoto to efficiently couple diarylamines with aryl halides to prepare triarylamines. Here we use (Pd(OAC)$_2$/P(*t*-Bu)$_3$/NaO*t*-Bu/toluene, 120 °C) reaction conditions and prepare the target isomers in 38–42% yield, respectively.

3.2. Crystal structure analysis

X-ray diffraction provided the final evidence for the isomers **1a** and **1b** (Fig. 2). The single crystals of isomers **1a** and **1b** were obtained from slow evaporation of its $CHCl_3$ solution at room temperature. For **2a** and **2b**, it was difficult to obtain crystals for X-ray analysis. Its crystal parameters are listed in Table 1, and selected crystal data are given in Table 2. The two molecules show some differences between them in the interplanar angles (θ) of the terminal rings: 81.9° (naphthalimide and phenyl C19–C24 rings), 71.4° (naphthalimide and phenyl C25–C30 rings), 62.9° (between the two phenyl rings) for the molecule **1a**, 83.7°, 68.3° and 64.9° for the molecule **1b**. It is noteworthy that, the central nitrogen atom (N3) and the three attached carbons are practically coplanar suggest that the nitrogen atom takes the sp^2 hybridization. The N3–C bond lengths for isomer **1a** are shorter than the bond lengths for isomer **1b** (Table 2), it is due to the larger conjugation between the arylamine group and the naphthalimide ring in **1a**. The molecular interactions (face to face packing) between the molecules in **1a** and **1b** crystals are as shown in Fig. 3, with the shortest interaction distances of 3.18 and 3.38 Å, respectively. This distance is close enough for π–π stacking interaction between the aromatic rings. No conventional hydrogen bonding is observed in those crystals.

3.3. Photophysical properties

The UV–vis absorption spectra of the systems have been studied in various solvents of different polarity and the spectral data have been collected in Table 3. A few representative spectra are shown in Fig. 4. As indicated in the absorption spectra, these derivatives reveal a common low-energy broad band at 450–490 nm assigned to an intramolecular charge transfer (CT) band from the arylamine group to the naphthalimide ring system in all solvents. This is evident from the following observations: 4-unsubstituted naphthalimides do not exhibit this band, and 4-amino-1,8-naphthalimide which possesses an electron-donating group at 4-position, displays a similar band [30–32]; the absorption is fairly broad and the peak position is rather sensitive to the polarity of the medium (vide Table 3). As a typical charge-transfer transition, an increase in the polarity of the medium leads to a Stokes shift of the absorption maximum. A change of the solvent from *n*-hexane to CH_2Cl_2 results in around 15 nm bathochromic shift of the absorption maximum. Compared with isomer **1b** (**2b**), the absorption spectra of isomer **1a** (**2a**) show consistent red-shift in the solvents of different polarity. As mentioned in the crystal structure analysis part, it was attributed to the longer effective conjugation length in **1a** (**2a**) than in **1b** (**2b**).

Table 3
Absorption and fluorescence data of **1a**–**2b** derivatives in different solvents at room temperature

Compd	Solvent	λ_{max}^{abs} (nm)	λ_{max}^{PL} (nm)	ϕ_f	τ_f	k_r (10^7 s^{-1})	k_{nr} (10^7 s^{-1})
1a	*n*-hex	474	530	0.821	10.10	8.12	1.78
	$CHCl_3$	479	570	0.205	4.85	7.19	27.89
	THF	480	585	0.089	1.06	8.40	85.94
	CH_2Cl_2	488	596	0.105	1.14	9.21	78.51
	ACN	481	602	0.051	1.49	3.42	66.78
1b	*n*-hex	455	497	0.780	9.87	7.90	2.23
	$CHCl_3$	460	548	0.185	4.21	7.09	31.23
	THF	462	578	0.080	0.86	9.30	106.98
	CH_2Cl_2	469	584	0.097	1.08	8.98	83.61
	ACN	462	586	0.042	1.12	3.75	88.93
2a	*n*-hex	479	539	0.523	5.66	9.19	8.48
	$CHCl_3$	483	582	0.107	2.26	4.73	39.51
	THF	484	591	0.077	0.98	7.86	94.18
	CH_2Cl_2	490	604	0.048	0.82	5.85	116.10
	ACN	485	606	0.020	0.97	2.06	102.89
2b	*n*-hex	460	510	0.479	5.50	8.73	9.45
	$CHCl_3$	465	553	0.082	2.03	4.04	45.22
	THF	465	580	0.052	0.72	7.22	131.67
	CH_2Cl_2	472	589	0.040	0.91	4.40	105.49
	ACN	468	592	0.015	0.85	1.76	117.53

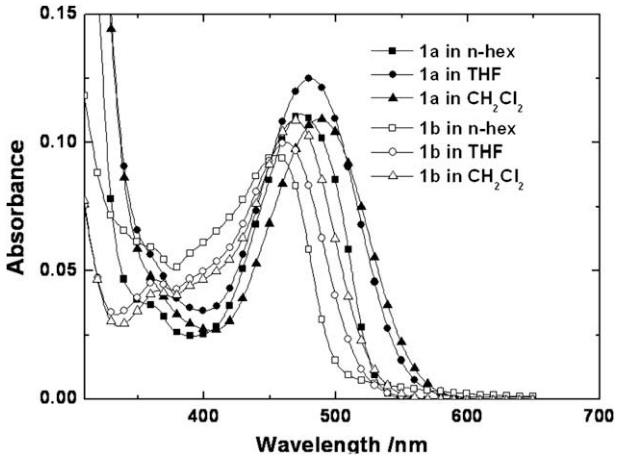

Fig. 4. Absorption spectra of **1a** and **1b** in *n*-hexane, THF and CH_2Cl_2.

Fluorescence spectra of the systems were recorded in various solvents of different polarity. The photoluminescent spectra of the systems consist of one broad band except in *n*-hexane, where some structure could be observed. The spectra of **1a**–**2b** show a large Stokes shift in more polar solvents, accompanied by losing of the fine structure and an increase in the fluorescence half-width. As an example, the normalized fluorescence spectra of **1a** and **1b** are shown in Fig. 5. As a change of the solvent from *n*-hexane to acetonitrile (ACN), the maximum emission wavelengths were red-shifted from 530 to 602 nm and 497 to 586 nm for **1a** and **1b**, respectively. The Stocks shifts for **1a**–**2b** are very large in polar solvents as compared to non-polar solvents indicating a considerable energetic stabilization of the excited state in polar solvents. Moreover, unlike the previously reported data of no difference in the absorption and PL of the similar isomeric mixture [33,34], the absorption and emission of isomer **1a** (**2a**) show consistent red-shift from isomer **1b** (**2b**). It was preliminarily confirmed by the results of quantum calculations on both compounds (vide part 4).

The solvent dependence of the fluorescence indicates that the excited state is stabilized in more polar solvents, as expected for an intramolecular CT. To obtain more information about the change in the dipole moment upon excitation, we used the Lippert–Mataga equation Eq. (1) [35,36], which expressed the Stokes shift as a function of the solvent polarity parameter $\Delta f(\varepsilon, n)$.

$$\upsilon_a - \upsilon_f = \left(2\Delta\mu^2/hca^3\right)\Delta f(\varepsilon, n) + C = 10,070\left(\Delta\mu^2/a^3\right)\Delta f(\varepsilon, n) + C \quad (1)$$

Where $\Delta f(\varepsilon, n)$ is calculated from Eq. (2):

$$\Delta f(\varepsilon, n) = [(\varepsilon - 1)/(2\varepsilon + 1)] - \left[\left(n^2 - 1\right)/\left(2n^2 + 1\right)\right] \quad (2)$$

In these relations, $\upsilon_a - \upsilon_f$ represents the Stokes shift (in cm^{-1}), where υ_a and υ_f are the spectral positions of the absorption maximum and solvent-equilibrated fluorescent maximum, respectively. $\Delta\mu$ is given by $\mu_e - \mu_g$, which is the magnitude of the change in the dipole moment from the ground state to the excited state. The other terms are: h corresponds to the Plank's constant (6.6×10^{-34} J s), c is the velocity of light in the vacuum (3.0×10^8 m s^{-1}) and a is the Onsager cavity radius (in meter), respectively. Onsager cavity radius was estimated from the optimized distance between the two farthest atoms in the direction of charge separation within the molecules, and the Onsager cavity radius a are set to 5.068 and 5.073 Å, as estimated from the crystallographic molecular volumes of **1a** and **1b**, projected onto a sphere of the same volume. Δf is the orientation polarizability parameter of the solvent where n is the refractive index of the medium and ε is the static dielectric constant of the solvent (both at room temperature). The Lippert–Mataga plot for **1a** and **1b** is shown in Fig. 6. From the slope of this plot, the difference of the dipole moment between the excited state and the ground state is estimated to be 8.97 and 9.65 D for **1a** and **1b**, respectively. This large change in dipole moment upon excitation is typical for photoinduced intramolecular CT processes.

Fluorescence quantum yields (ϕ_f) of the systems, measured in a series of solvents of different polarity, are collected in Table 3. As shown in the table, overall the four derivatives show high fluorescence quantum yields in non-polar solvents and the values decrease as the solvent polarity increases indicating strong quenching from dipole–dipole interaction of the solvent and the solute molecules. The decrease is most prominent in a polar environment. The influence of the amino group on the fluorescence efficiency of the systems is clearly evident from the data presented in Table 3. In all media, the yield decreases as the size containing the arylamino nitrogen is increased.

The fluorescence decay behaviors of the systems have been studied in several solvents of different polarity and the data have been presented in Table 3. Typical decay profiles are shown in Fig. 7. All the four derivatives exhibit single-exponentical decay in all

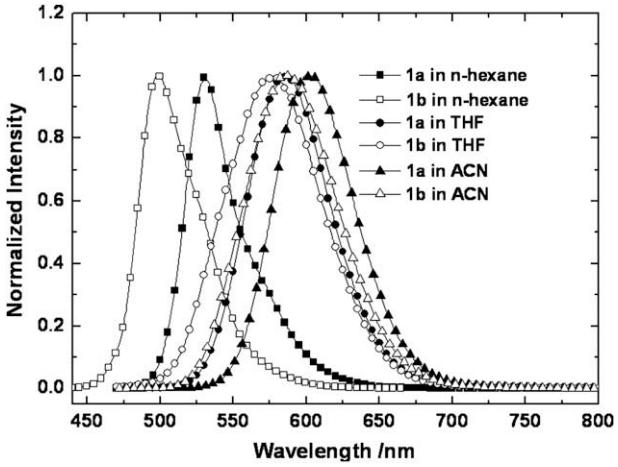

Fig. 5. Fluorescence spectra of **1a** and **1b** in *n*-hexane, THF and ACN.

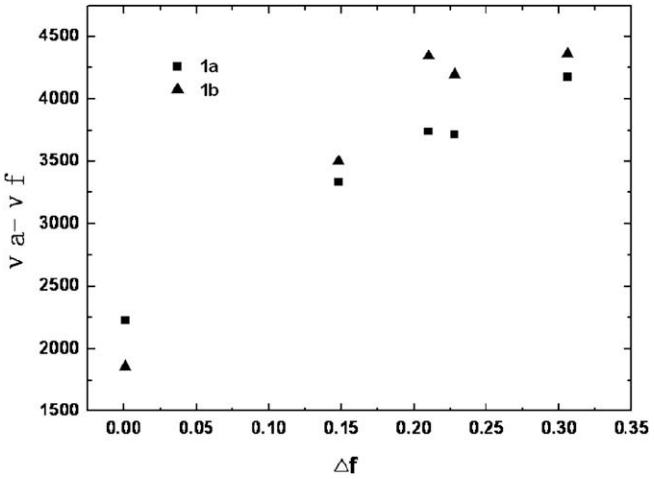

Fig. 6. Lippert–Mataga plot for the **1a** and **1b**.

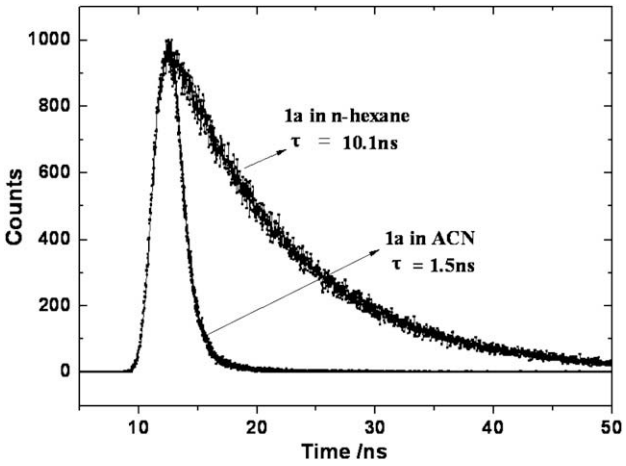

Fig. 7. Fluorescence decay curves for **1a** in *n*-hexane and ACN.

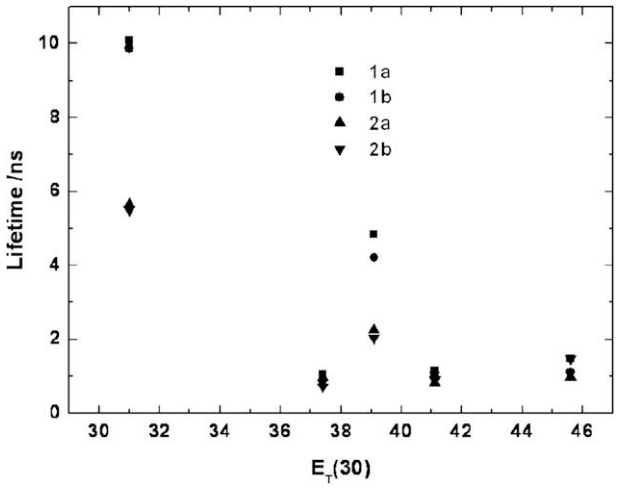

Fig. 8. Plots of measured emission lifetime of **1a**–**2b** vs $E_T(30)$.

solvents irrespective of the polarity. Even in ACN, a single-exponential behavior is observed. As shown in Table 3, the effect of polarity is very similar to what is observed for the fluorescence quantum yield, increase in the polarity of the medium leads to a shortening of the lifetime; for instance, **1a** has a lifetime of 10.1 ns in *n*-hexane and 1.5 ns in ACN. This is further clearly shown in the plot of lifetime vs $E_T(30)$ in Fig. 8; $E_T(30)$ is another commonly used parameter denoting the polarity of a solvent [37]. These data indicate that the excited moleculars are quenched efficiently by polar solvents and the quenching should be due to the dipole–dipole interaction between solvent and solute.

The radiative (k_r) and nonradiative (k_{nr}) rate constants of the systems in different solvents, evaluated from the measured values of ϕ_f and τ_f using $\kappa_r = \phi_f/\tau_f$ and $\kappa_{nr} = (1-\phi_f)/\tau_f$, are collected in Table 3. These values can be regarded as crude estimation, since the measurement of ϕ_f and τ_f is not very accurate. As can be seen, the radiative rate constants of the systems do not depend on the nature of the medium. Instead, these values cluster within a narrow range, except for the fact that these values are relatively lower in ACN. Even though the polarity of the medium has very little influence on the k_r values, the effect of the medium is rather dramatic on the k_{nr} values. In **1a** and **1b**, nearly 40-fold increase in the nonradiative rate constant could be observed on changing the solvent from *n*-hexane to ACN. The difference in the k_{nr} values of the systems because of a difference in the rate of some internal motion in the molecular systems is attributed to an internal rotation (twisting) around the C–N bond or an inversion of the amino nitrogen [38].

4. Quantum chemical calculation

Quantum chemical calculations based on density functional theory (DFT) are performed in order to understand the energy levels and to explain the transitions of observed absorption and emission spectra of **1a** and **1b**. The optical geometry of the ground state for **1a** and **1b** using method B3LYP at basis set 6-31G* is obtained and is shown in Fig. 9. Vibrational frequencies were calculated to ensure no imaginary frequency existing for these structures. Bond lengths and bond angles resulting from the X-ray

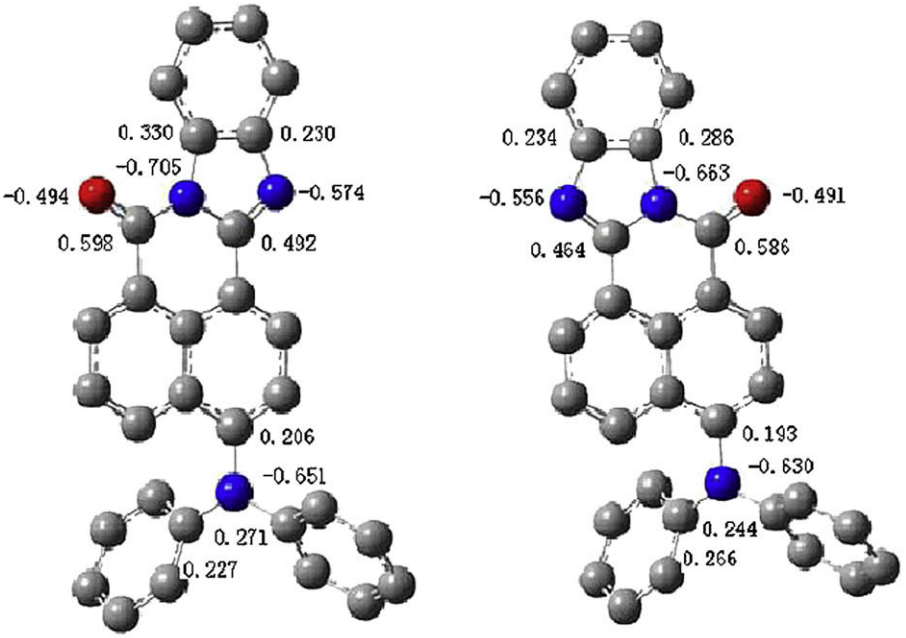

Fig. 9. Optimized structures for **1a** and **1b** based on method B3LYP/6-31G*.

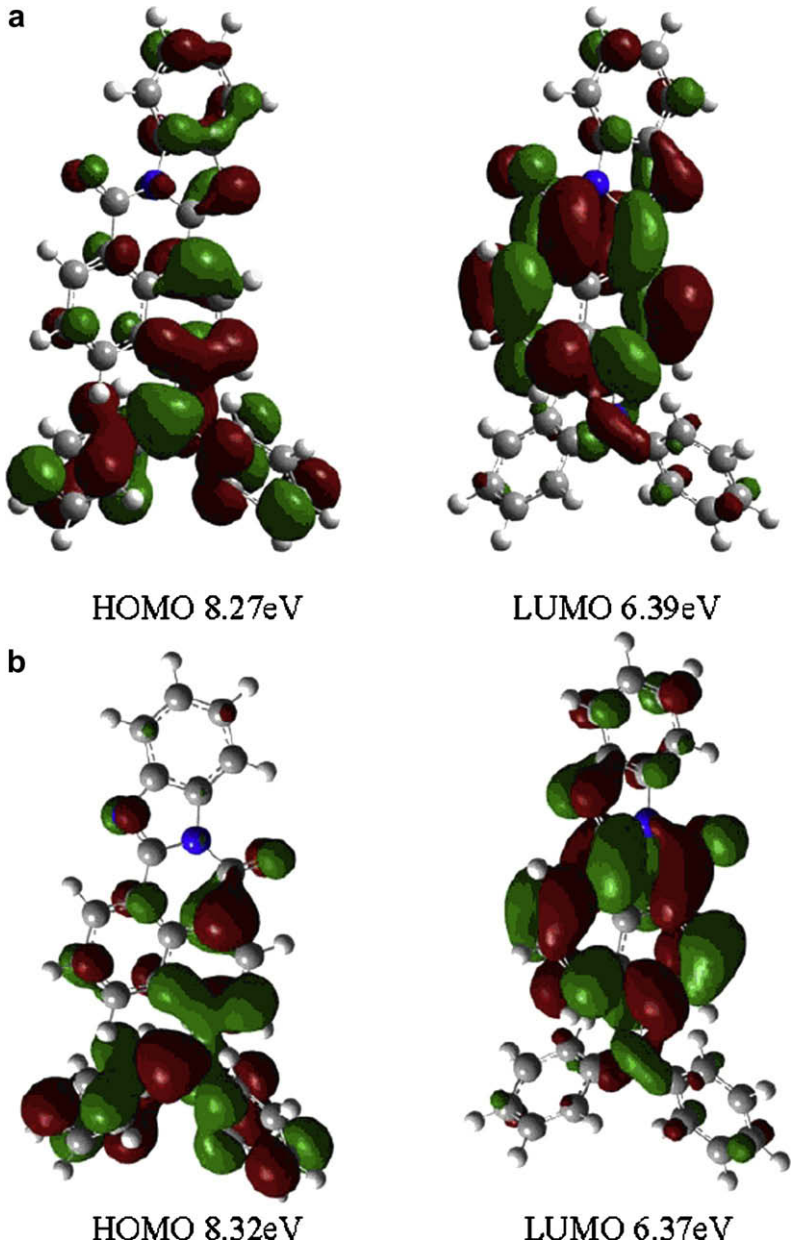

Fig. 10. Frontier orbitals of compounds **1a** and **1b** calculated by the B3LYP/6-31G* DFT method.

data are compared to those obtained from quantum chemical calculations. The data agree excellently for both molecules, and deviations are generally smaller than 2%. As shown in Fig. 9, the three aromatic planes are twisted to each other and the BBI moiety has a planar geometry. From the calculated charge distribution, the center nitrogen atom carries a negative partial charge and carbon atoms bonded to it with positive partial charge, yielding small net dipole from this part. On the BBI moiety, oxygen atom and two nitrogen atoms are with negative partial charge and carbons are with the opposite charge resulting in a dipole of 4.48 and 3.62 D (B3LYP/6-31G*) for **1a** and **1b**, respectively. Time-dependent DFT (TD-DFT) calculation yields the first vertical transition S_1–S_0 of **1a** and **1b**, a HOMO to LUMO excitation at wavelength 519 and 480 nm with an oscillator strength of 0.2783 and 0.3170, respectively. Based on the one electron LUMO and HOMO characteristics, this transition involves the π electron on the nitrogen atom and phenyl plane to the π^* orbital in the BBI moiety. The calculated energy for vertical excitation of the lowest energy band is about 8% lower than the experimental value in *n*-hexane solution. The isodensity surface plots of HOMO and LUMO are shown in Fig. 10. Moreover, the HOMO–LUMO energies of **1a** are different from those of **1b**. While in **1b** most of HOMO is delocalized on the diphenylamine and naphthalene rings, in **1a** the HOMO shows better distributed over the whole molecular skeleton. The HOMO–LUMO gap shows a decrease when going from **1b** to **1a**, which correlates well with the observed bathochromic shift.

5. Conclusions

In summary, four new isomers **1a**–**2b** were synthesized in good yields by palladium-catalyzed condition and crystal structures of two compounds **1a** and **1b** were determined. In addition, the absorption and photoluminescent spectra of the systems in several solvents of different polarity were investigated. A large Stokes shift in these intramolecular CT compounds was observed in polar solvents. The absorption and emission of isomer **1a** (**2a**)

show consistent red-shift from isomer **1b** (**2b**), and the theoretical results are in good agreement with experimental data.

6. Supplementary material

Crystallographic data for the structures (**1a** and **1b**) in this paper have been deposited with the Cambridge Crystallographic Data Centre as supplemental publications CCDC 661251 and 661252. Copies of the data can be obtained, free of charge, on application to CCDC, 12 Union Road, Cambridge CB2 1EZ, UK (fax: +44 0 1223 336033 or e-mail: deposit@ccdc.cam.ac.uk).

Acknowledgements

The support of this research by the National 973 Fund (2007CB936300) and the High-Technique Project Foundation of Jiangsu Province (BG 2005034) is gratefully acknowledged.

References

[1] Bredas JL, Beljonne D, Coropceanu V. Charge-transfer and energy-transfer processes in pi-conjugated oligomers and polymers: a molecular picture. Chem Rev 2004;104(11):4971–5003.
[2] Zhang QT, Tour JM. Alternating donor/acceptor repeat units in polythiophenes. Intramolecular charge transfer for reducing band gaps in fully substituted conjugated polymers. J Am Chem Soc 1998;120(22):5355–62.
[3] Pal SK, Bhattacharaya S, Batabyal SK. Role of TiO2 nanoparticles on the photoinduced intramolecular electron-transfer reaction within a novel synthesized donor–acceptor system. J Photochem Photobiol A 2007;189(1):86–93.
[4] Misra R, Kumar R, Prabhuraja V, Chandrashekar TK. Modified push–pull expanded corroles: syntheses, structure and nonlinear optical properties. J Photochem Photobiol A 2005;175(2–3):108–17.
[5] Yang CJ, Jenekhe SA, Meth JS. Probing structure–property relationships in third-order nonlinear optical polymers: third harmonic generation spectroscopy and theoretical modeling of systematically derivatized conjugated aromatic polyimines. Ind Eng Chem Res 1999;38(5):1759–74.
[6] Alam MM, Jenekhe SA. Nanolayered heterojunctions of donor and acceptor conjugated polymers of interest in light emitting and photovoltaic devices: photoinduced electron transfer at polythiophene/polyquinoline interfaces. J Phys Chem B 2001;105(13):2479–82.
[7] Jenekhe SA, Yi S. Efficient photovoltaic cells from semiconducting polymer heterojunctions. Appl Phys Lett 2000;77(17):2635–7.
[8] Islam A, Cheng CC, Cheng CH. Aminonaphthalic anhydrides as red-emitting materials: electroluminescence, crystal structure, and photophysical properties. J Phys Chem B 2005;109(12):5509–17.
[9] Gan JA, Song QL, Hou XY, Chen KC, Tian H. 1,8-Naphthalimides for non-doping OLEDs: the tunable emission color from blue, green to red. J Photochem Photobiol A 2004;162(2–3):399–406.
[10] Zhu WH, Hu M, Yao R, Tian H. A novel family of twisted molecular luminescent materials containing carbazole unit for single-layer organic electroluminescent devices. J Photochem Photobiol A 2003;154(2–3):169–77.
[11] Martynski T, Mykowska K, Bauman D. Spectral properties of fluorescent dyes in nematic liquid crystals. J Mol Struct 1994;325(8):161–7.
[12] Schon JH, Kloc C, Dodabalapur A, Batlogg B. An organic solid state injection laser. Science 2000;289(5479):599–601.
[13] Niemz A, Rotello VM. Modification of spin density distribution via specific hydrogen bond interactions: an experimental, UHF, and density functional study. J Am Chem Soc 1997;119(29):6833–6.
[14] Wong MS, Li ZH, Tao Y, Iorio MD. Synthesis and functional properties of donor–acceptor -conjugated oligomers. Chem Mater 2003;15(5):1198–203.
[15] Loi MA, Denk P, Hoppe H, Neugebauer H, Winder C, Meissner D, et al. Long-lived photoinduced charge separation for solar cell applications in phthalocyanine–fulleropyrrolidine dyad thin films. J Mater Chem 2003;13(4):700–4.
[16] Ramesh KK, Martin P, Ronald LE. A simple method for fabricating polymeric light-emitting diodes. Chem Mater 1998;10(1):235–7.
[17] Thomas KRJ, Lin JT, Tao YT. Quinoxalines incorporating triarylamines: potential electroluminescent materials with tunable emission characteristics. Chem Mater 2002;14(6):2796–802.
[18] Yu MX, Duan JP, Lin CH. Diaminoanthracene derivatives as high-performance green host electroluminescent materials. Chem Mater 2002;14(9):3958–63.
[19] Zhao HD, Tanjutco C, Thayumanavan S. Design and synthesis of stable triarylamines for hole-transport applications. Tetrahedron Lett 2001;42(27):4421–4.
[20] DeSilva AP, Gunaratne HQN, Gunnlaugsson T, Huxley AJM, McCoy CP, Rademacher JT, et al. Signaling recognition events with fluorescent sensors and switches. Chem Rev 1997;97(5):1515–66.
[21] Grabchev I, Guittonneau S. Sensors for detecting metal ions and protons based on new green fluorescent poly(amidoamine) dendrimers peripherally modified with 1,8-naphthalimides. J Photochem Photobiol A 2006;179(1–2):28–34.
[22] Grabchev I, Chovelon JM, Nedelcheva A. Green fluorescence poly(amidoamine) dendrimer functionalized with 1,8-naphthalimide units as potential sensor for metal cations. J Photochem Photobiol A 2006;183(1–2):9–14.
[23] Bojinov V, Grabchev I. Novel functionalized 2-(2-hydroxyphenyl)-benzotriazole – benzo[*de*]isoquinoline-1,3-dione fluorescent UV absorbers: synthesis and photostabilizing efficiency. J Photochem Photobiol A 2005;172(3):308–15.
[24] Bojinov V, Grabchev I. Synthesis of new polymerizable 1, 8-naphthalimide dyes containing a 2-hydroxyphenylbenzotriazole fragment. Dyes Pigments 2003;59(3):277–83.
[25] Jiang W, Sun YM. Synthesis and photochemical properties of novel 4-diarylamine-1,8-naphthalimide derivatives. Dyes Pigments 2008;77(1):125–8.
[26] Stieter ER, Blackmond DG, Buchwald SL. Insights into the origin of high activity and stability of catalysts derived from bulky, electron-rich monophosphinobiaryl ligands in the Pd-catalyzed C–N bond formation. J Am Chem Soc 2003;125(46):13978–90.
[27] Yamamoto T, Nishiyama M. Palladium-catalyzed synthesis of triarylamines from aryl halides and diarylamines. Tetrahedron Lett 1998;39(25):2367–70.
[28] Bickelhaupt FM, Baerends EJ. Kohn–Sham density functional theory: predicting and understanding chemistry. Rev Comput Chem 2000;15:1–86.
[29] Crayshan PH, Peters AT. Heterocyclic derivation of naphthalene-1,8-dicarboxylic anhydride. Part 1. Nitro-7*H*-benzimidazo[2,1-*a*]benz[*de*]isoquinolin-7-ones. J Heterocycl Chem 1973;10(1):699–703.
[30] Elbrt JE, Paulsen S, Robinson L, Elzey S. A study of 4-(alkylamino)amino substituted 1,8-naphthalimide fluoroionophores. J Photochem Photobiol A 2005;169(1):9–19.
[31] Bojinov V, Konstantinova T. Synthesis of polymerizable 1,8-naphthalimide dyes containing hindered amine fragment. Dyes Pigments 2002;54(3):239–45.
[32] Khosravi A, Moradian S, Gharanjig K, Taromi FA. Synthesis and spectroscopic studies of some naphthalimide based disperse azo dyestuffs for the dyeing of polyester fibres. Dyes Pigments 2006;69(1–2):79–92.
[33] Zhu WH, Yao R, Tian H. Synthesis of novel electro-transporting emitting compounds. Dyes Pigments 2002;54(2):147–54.
[34] Qian XH, Ren SW. Benzoxanthene-3,4-dicarboximides and benzimidazoxantheno isoquinolinones. J Chem Eng Data 1988;33(4):528–9.
[35] Sumalekshmy S, Gopidas KR. Photoinduced intramolecular charge transfer in donor–acceptor substituted tetrahydropyrenes. J Phys Chem B 2004;108(12):3705–12.
[36] Mataga N, Kaifu Y, Koizumi M. Solvent effects upon fluorescence spectra and the dipolemoments of excited molecules. Bull Chem Soc Jpn 1956;29(4):465–71.
[37] Reichardt C. Solvents and solvent effects in organic chemistry. 2nd ed. Weinheim: VCH; 1988.
[38] Saha S, Samanta A. Influence of the structure of the amino group and polarity of the medium on the photophysical behavior of 4-amino-1,8-naphthalimide derivatives. J Phys Chem A 2002;106(18):4763–71.